Vol 18 No 12, December 2009
1674-1056/2009/18(12)/5523-11

Chinese Physics B

© 2009 Chin. Phys. Soc.
and IOP Publishing Ltd

Improved anti-Stokes energy transfer between rare earth ions in Er(0.5)Yb(9.5):FOV oxyfluoride vitroceramics explains the strong color reversal*

Chen Xiao-Bo(陈晓波)[a)†], Wang Ce(王 策)[a)], Gregory J. Salamo[b)], Naruhito Sawanobori[c)], Kang Dong-Guo(康栋国)[d)], Masaaki Ohtsuka[c)], Yang Guo-Jian(杨国建)[a)e)], and Peng Fang-Lin(彭芳麟)[a)e)]

[a)] *Applied Optics Beijing Area Major Laboratory, Beijing Normal University, Beijing* 100875, *China*
[b)] *University of Arkansas, Department of Physics, Fayetteville, AR* 72701, *USA*
[c)] *Sumita Optical Glass, Inc.,* 4-7-25 *Harigaya, Urawa, Saitama, 338, Japan*
[d)] *Beijing Institute of Applied Physics and Computational Mathematics, Beijing* 100088, *China*
[e)] *Applied Optics Beijing Area Major Laboratory and Physics Department, Beijing Normal University, Beijing* 100875, *China*

(Received 30 May 2009; revised manuscript received 22 July 2009)

The widely used energy transfer theory is a foundation of luminescence, in which the rates of Stokes and anti-Stokes processes have the same calculation formula. An improvement on the anti-Stokes energy transfer to explain the fluorescence intensity reversal between the red and green fluorescence of Er(0.5)Yb(9.5):FOV is reported in the present article. The range of the intensity reversal Σ was measured to be 877. Dynamic processes for 16 levels were simulated. A coefficient, the improvement factor of the intensity ratio of Stokes to anti-Stokes processes in quantum Raman theory compared to classical Raman theory, is introduced to successfully describe the anti-Stokes energy transfer. A new method to calculate the distance between the rare earth ions, which is critical for the energy transfer calculation, is proposed. The validity of these important improvements is also proved by experiment.

Keywords: improvement of anti-Stokes energy transfer, nanomaterial, $Er^{3+}Yb^{3+}$ co-doped rare earth ion material

PACC: 7855, 4270, 7820

1. Introduction

Photons feature many distinct capacities. Photonics has exhibited an increasingly competitive power that has redounded to the development of modern science and technology due to its exceedingly fast response speed, extremely large information capacity and tremendously high information efficiency.[1−3] As a frontier of science, multiphoton photonics has already achieved a great deal of success in multiphoton imaging and microscopy. Additionally, it has played a vital role in multiphoton spectroscopy, three-dimensional (3D) controlling and micro-processing, 3D optical storage and so forth. Photonics has become an important new mainstay in modern science.[1−3] Moreover, nanomaterial and nanostructure research has led to new knowledge of nature and science.[4] The human probing ability has expanded to the media field between microscopic and macroscopic objects.[1,2] One of the most important tasks nowadays is to study thoroughly the properties, structures, and especially the optical spectroscopic features of nanomaterials, to find out their special physical law by comparison with common materials, and to establish new concepts and new theories appropriate to the described nanomaterials.[4] Therefore, research into the multiphotonics of nano rare earth materials is invaluable and urgent, and holds promise for excellent application prospects, which is a probe of the present manuscript.

The present paper deals with an interesting photonic phenomenon, the fluorescence intensity reversal between the red and green fluorescence of $Er^{3+}Yb^{3+}$ co-doped nanophase oxyfluoride vitroceramic Er(0.5)Yb(9.5):FOV.[5−7] First, all basic data,

*Project supported by the National Natural Science Foundation of China (Grant No 10674019).
†Corresponding author. E-mail: xbchen@bnu.edu.cn

like spontaneous emission rates, energy transfer rates, back energy transfer rates, multiphonon relaxation rates, the stimulated emission rates and the stimulated absorption rates at 0.3 mW experimental pumping power, are measured and calculated carefully. Then, a new method, based on crystal structure and the stoichiometric method, is proposed to calculate the distance R between rare earth ions more accurately. As we know, in energy transfer theory,[8] the rate of energy transfer is sensitive to the distance between the donor and the acceptor. The conventional general methods for calculating the distance between the ions[9−11] may cause imprecise descriptions especially for a nanomaterial in which the distance R is much smaller than that in a normal material. In this paper, the new method proposed by us can be used to calculate the distance between the rare earth ions in the nanophase Er(0.5)Yb(9.5):FOV more precisely, and can also be used for reference in other materials. Finally, it is found in our paper that, under the unchanged good Kushida theory,[8] the original phonon-assistant rare earth ion energy transfer theory[12,13] cannot explain the observed experimental results well as it does not take into account the difference between Stokes and anti-Stokes processes. It is just like the well-known quantum Raman scattering theory which makes an important improvement to the classical Raman scattering theory to take into account the difference between the Stokes and anti-Stokes processes sufficiently in order to describe them perfectly. The additional proportion coefficient between the Stokes and anti-Stokes light intensity of quantum Raman scattering theory[7] as compared to the classical Raman theory is introduced into the widely used theory of rare earth ion energy transfer to successfully describe the anti-Stokes energy transfer in this paper. Generally, the dynamics of all 16 levels of relative materials, when induced by 378.5 nm and 522.3 nm light, were calculated numerically. Also, the population dynamical processes of all Er^{3+} ion levels within 30000 cm^{-1} were analyzed carefully.[14] The results of theoretical numerical calculations with our improved energy transfer theory coincide very well with the experimental results.

2. Sample

The oxyfluoride glass samples were made from silicon oxide SiO_2 and the fluorides of lead PbF_2, zinc ZnF_2, lutetium LuF_3, ytterbium YbF_3, and erbium ErF_3. All the raw materials were highly pure reagents and were put into a platinum crucible for heating at about 900 °C for 100 minutes. Then they were cooled fast at an iron plate to form oxyfluoride glass. The oxyfluoride vitroceramics was obtained by annealing at the glass transition temperature for 7 hours.[15−19] The size of the nanocrystalline is about 19 nm. It is transparent. The optical scattering loss in the visible and infrared wavelength range is very small. The optical scattering loss in the ultraviolet edges is slightly larger than the oxyfluoride glass sample. The composition of the sample Er(0.5)Yb(9.5):FOV, as an example, is 9.5% YbF_3, 0.5% ErF_3, 30% PbF_2, 15% ZnF_2, and 45% SiO_2. As is known, oxyfluoride vitroceramics is composed of a proportion of the cubic structure β-PbF_2 and a proportion of residual glass.[16] If the crystallized volume ratio η is defined as the proportion of the volume between the cubic structure β-PbF_2 and whole oxyfluoride vitroceramics, it is found by relative research that the crystallized volume ratio η of oxyfluoride vitroceramics is positioned in a range of 2% to 30%.[16,18,19]

3. Experiments

Fluorescence spectra of Er^{3+} doped nanophase oxyfluoride vitroceramics were measured by using a fluorescence spectrophotometer equipped with a double-grating monochromator (JY-ISA, Fluorolog-Tau-3).[5,6] According to the Stokes excitation spectrum, two relatively strong excitation peaks at 378.5 nm and 522.3 nm, corresponding to the $^4G_{11/2}$ and $^2H_{11/2}$ levels of the Er^{3+} ion respectively,[14,17] were observed. Then the Stokes emission spectra of the samples under the excitation at these two wavelengths were studied. Obvious emission peaks around 411.1 nm, 551.1 nm and 667.1 nm were observed, corresponding to the fluorescence emission of $(^2G^4F^2H)_{9/2} \rightarrow {}^4I_{15/2}$, $^4S_{3/2} \rightarrow {}^4I_{15/2}$ and $^4F_{9/2} \rightarrow {}^4I_{15/2}$, respectively.[14,17] We find that the fluorescence of $^4S_{3/2} \rightarrow {}^4I_{15/2}$ is stronger than that of $^4F_{9/2} \rightarrow {}^4I_{15/2}$ when the Er(0.5)Yb(9.5):FOV is excited by 522.3 nm light, but the fluorescence strengths

of 551.1 nm green and 667.1 nm red light reverse when the sample is excited by 378.5 nm ultraviolet light. However, this is not the case when we do the same experiment for Er(0.5):FOV in which the fluorescence intensity of $^4S_{3/2} \rightarrow {}^4I_{15/2}$ is always stronger than that of $^4F_{9/2} \rightarrow {}^4I_{15/2}$ with a similar ratio. A common intensity ratio α can be defined as the ratio of green fluorescence intensity $I(^4S_{3/2})$ to red fluorescence intensity $I(^4F_{9/2})$ when the $^2H_{11/2}$ level is excited at 522.3 nm. An unusual intensity reversal ratio γ is also defined, which is equal to the ratio of $I(^4F_{9/2})$ to $I(^4S_{3/2})$ when excited by 378.5 nm light. Thus the range of intensity reversal Σ can be expressed by $\Sigma = \alpha \times \gamma$. The experimental value of Σ for Er(0.5):FOV is 0.9320. But for Er(0.5)Yb(9.5):FOV, the range of intensity reversal Σ is 877 due to the obvious fluorescence intensity reversal phenomenon. Meanwhile the same experiments for Er(0.05)Yb(9.5):FOV are done for comparison, when we discuss the new method to calculate the distance between rare earth ions precisely. The range of intensity reversal Σ for Er(0.05)Yb(9.5):FOV is 846, which is similar to the value in Er(0.5)Yb(9.5):FOV. Detailed calibrated results and a schematic energy level diagram are shown in Table 1, Fig.1 and Fig.2 respectively.

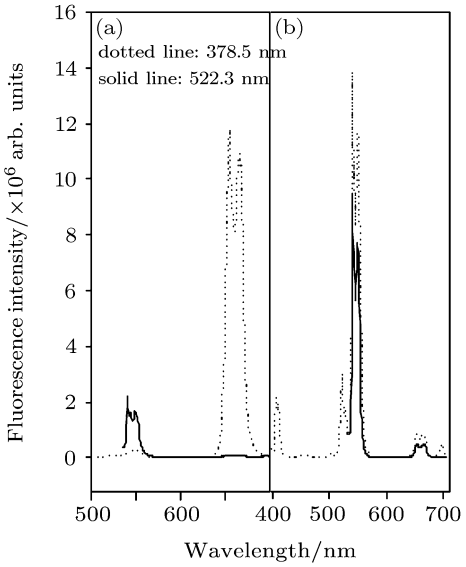


Fig.1. Experimental calibrated fluorescence spectra of the fluorescence intensity reversal. The fluorescence emission spectra excited by 378.5 nm and 522.3 nm light sources for Er(0.5)Yb(9.5):FOV (a) and Er(0.5):FOV (b).

Table 1. Experimental and numerical calculation results of the fluorescence intensity reversal phenomenon.

sample	$I(^4S_{3/2})/^2H_{11/2}$	$I(^4S_{3/2})/^4G_{11/2}$	$I(^4F_{9/2})/^2H_{11/2}$	$I(^4F_{9/2})/^4G_{11/2}$	α	γ	Σ
1 ^{e}	2.057×10^{7}	4.216×10^{6}	1.204×10^{6}	2.165×10^{8}	1.709×10^{1}	5.135×10^{1}	8.776×10^{2}
2 ^{e}	1.039×10^{8}	1.901×10^{8}	9.497×10^{6}	1.618×10^{7}	1.095×10^{1}	8.511×10^{-2}	9.319×10^{-1}
3 ^{e}	1.781×10^{6}	7.005×10^{5}	9.839×10^{4}	3.273×10^{7}	1.810×10^{1}	4.672×10^{1}	8.456×10^{2}
1–10% ^{tn}	1.829×10^{-2}	1.155×10^{-2}	3.090×10^{-2}	1.216×10^{-1}	5.920×10^{-1}	1.053×10^{1}	6.232×10^{0}
1–16% ^{tn}	6.580×10^{-2}	7.645×10^{-3}	1.814×10^{-2}	1.953×10^{-1}	3.628×10^{0}	2.555×10^{1}	9.269×10^{1}
1–22.6% ^{tn}	1.524×10^{-1}	6.393×10^{-3}	2.343×10^{-2}	2.756×10^{-1}	6.504×10^{0}	4.311×10^{1}	2.804×10^{2}
1–10% ^{ti}	1.358×10^{-2}	6.099×10^{-6}	2.142×10^{-3}	3.775×10^{-1}	6.339×10^{0}	6.189×10^{4}	3.923×10^{5}
1–16% ^{ti}	6.542×10^{-2}	3.064×10^{-4}	1.058×10^{-2}	3.907×10^{-1}	6.185×10^{0}	1.275×10^{3}	7.885×10^{3}
1–22.6% ^{ti}	1.550×10^{-1}	2.701×10^{-3}	2.524×10^{-2}	3.896×10^{-1}	6.141×10^{0}	1.442×10^{2}	8.857×10^{2}
2 ^{ti}	8.337×10^{-1}	8.152×10^{-1}	1.365×10^{-1}	1.355×10^{-1}	6.108×10^{0}	1.662×10^{-1}	1.015×10^{0}
3 ^{ti}	1.584×10^{-1}	2.857×10^{-3}	2.580×10^{-2}	3.895×10^{-1}	6.141×10^{0}	1.363×10^{2}	8.370×10^{2}

In Table 1, in the sample column, the numbers 1–3 represent Er(0.5)Yb(9.5):FOV, Er(0.5):FOV, and Er(0.05)Yb(9.5):FOV respectively. Lines 2–4 are the experimental calibrated results marked by the superscript 'e'. Lines 5–7 are the results calculated with the original theory marked by the superscript 'tn'. Lines 8–12 are the results calculated with the improved theory marked by the superscript 'ti'. The percentage after the sample's number represents the total crystallized volume ratio in the vitroceramics. From the second column to the fifth column, the data are the measured fluorescence intensity or steady values of I/N for the theoretically calculated results, and the levels to the right of the slant correspond to directly excited levels. α, γ, Σ are the common intensity ratio, unusual intensity reversal ratio, and the range of intensity reversal respectively, and are defined in the text.

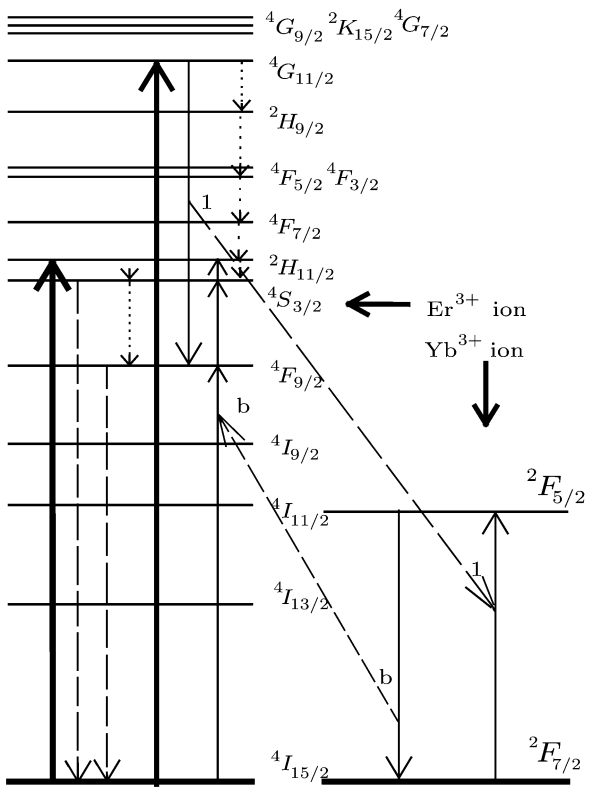


Fig.2. A schematic diagram of the energy level structure of Er^{3+} and Yb^{3+} ions. The 1–1 line represents the main energy transfer which results in the strong color reversal. The b–b line represents the key anti-Stokes back energy transfer.

4. Numerical calculation method

A rate equation was firstly set up to depict the dynamic processes of the whole system. Interactions between three and more ions were ignored here. Then the rate equations governing the transitions between different energy states of rare earth ions can be written as

$$\frac{\mathrm{d}n_i}{\mathrm{d}t} = \sum_{s,p}\Bigg\{\sum_{j,m,n,k}[W_s^{(j\to i)}\cdot n_j + W_p^{(m\to n,k\to i)}\cdot n_m n_k] - \sum_{j,m,n,k}[W_s^{(i\to j)}\cdot n_i + W_p^{(m\to n,i\to k)}\cdot n_m n_i]\Bigg\}, \quad (1)$$

where n_i is the population probability of level i which means the probability positioned at level i for one rare earth ion; $W_s^{(j\to i)}$ denotes the transition rate of single ions from level j to i, $W_p^{(m\to n,k\to i)}$ is the probability of interactions, including energy transfer and back energy transfer processes,[8,12,13] m and k denote the initial levels of two ions, n and i stand for the final levels. In this paper, as the absorption peaks from $^4I_{15/2}\to{}^4I_{13/2}$ to $^4I_{15/2}\to{}^2K_{15/2}$ in the absorption spectra can be measured, fourteen levels of erbium will be considered. So the formula (1) includes 14 equations that are sufficient for Er(0.5):FOV. To discuss Er(0.5)Yb(9.5):FOV and Er(0.05)Yb(9.5):FOV, however, another set of equations are needed to describe the ytterbium ions. Nearly 600 rate data, like the spontaneous emission rates obtained from Judd–Ofelt three intensity parameters,[17] nonradiative multiphonon relaxation rates calculated from the lifetime of energy levels and theory by Miyakawa and Dexter,[8,12,13] energy transfer rates and back energy transfer rates obtained from the theory of Kushida, Miyakawa and Dexter,[8,12,13] the stimulated emission rates and the stimulated absorption rates at 0.3 mW experimental pumping power,[17] are used to calculate formula (1). In this paper we focus on the simulation of an intensity reversal phenomenon where energy transfer plays an important role. In order to conveniently discuss our work in the calculation of distance between the ions and the confirmation of improvement based on original energy transfer theories, the values of some important energy transfer transitions are listed in Table 3. An analytic solution of the equations is hard to reach, so a numerical method will be adopted. Considering that the time variable Δt is small enough, equation (2) is tenable. The initial condition is 1 for the ground level and 0 for the excited levels. Curves of each level's population probabilities vs. time will be obtained, and finally the data after stabilization will be taken as the solution of the equations

$$n(t+\Delta t) = n(t) + \Delta t\cdot \mathrm{d}n/\mathrm{d}t. \quad (2)$$

5. Calculation of distance between interacting ions

Note that the phenomenon of the intensity reversal between red and green fluorescence has an inseparable relation to the doping Yb^{3+} ions in the materials. Also, the energy transfer and back energy transfer between Er^{3+} and Yb^{3+} ions are a very decisive factor in this phenomenon.[5,6] On the basis of Kushida's theory,[8] the rate of energy transfer W_{ET} is sensitive to the distance R between the interacting ions. So a correct definition of the distance between rare earth ions is important to the explanation of the phenomenon. Because W_{ET} decreases rapidly as R increases, we usually adopt the nearest distance between

the nearest neighbor rare earth ions in the calculation. Generally we consider that the rare earth ions are basically distributed uniformly in the materials. Although the number N of rare earth ions per unit volume is a key parameter in most methods to define R, the actual calculation processes are usually different.[9−11] For a stoichiometric material, the formula to calculate the real ion distance is

$$R^3 = R_0^3 \cdot (1/q), \tag{3}$$

where R_0 is the distance between the nearest ions in the unit cell and q is the concentration. The formula (3) is widely used and has been proved to be correct. For a rare earth ion co-doped material, there are two main methods. One[10] is

$$R^3 = \frac{6}{\pi} \cdot \left(\frac{1}{N_{\mathrm{D}} \cdot N_{\mathrm{A}}}\right)^{1/2}. \tag{4}$$

Another method for cubic structure, volume-center cubic structure and surface-center cubic structure[9,11] is shown in the following formula of Eqs.(5), (6) and (7)

$$R^3_{\mathrm{cubic}} = 0.62^3 \cdot \left(\frac{1}{N_{\mathrm{D}} + N_{\mathrm{A}}}\right), \tag{5}$$

$$R^3_{\mathrm{bcc}} = 0.62^3 \cdot \left(\frac{2}{N_{\mathrm{D}} + N_{\mathrm{A}}}\right) \times \left(\frac{\sqrt{3}}{2}\right)^3, \tag{6}$$

$$R^3_{\mathrm{fcc}} = 0.62^3 \cdot \left(\frac{4}{N_{\mathrm{D}} + N_{\mathrm{A}}}\right) \times \left(\frac{\sqrt{2}}{2}\right)^3. \tag{7}$$

In this manuscript, the following formula (8), for the rare earth ions in PbF_2 crystalline, is proposed by us from the formula of the stoichiometric material and unit cell of the crystal structure

$$R^3 = 1.061 \cdot \left(\frac{2}{N_{\mathrm{D}} + N_{\mathrm{A}}}\right). \tag{8}$$

The obtained calculation results coincide with experiments very well. This method would greatly benefit the calculation of energy transfer rates and can be extended to the calculation of non-full concentration materials.

We suppose N_{D} to be the number density of energy donors and N_{A} the number density of energy acceptors. It is clear for single-doped stoichiometric material that the average number density of rare earth ions is $\overline{N} = N = (N_{\mathrm{D}} + N_{\mathrm{A}})/2$ because the donor and acceptor are the same kind of ion. So for double-doped stoichiometric material, the average number density of rare earth ions is also $(N_{\mathrm{D}} + N_{\mathrm{A}})/2$ and the average volume of each rare earth ion equals $\overline{V} = 2/(N_{\mathrm{D}}+N_{\mathrm{A}})$.

For the crystal material, we can calculate the volume of each rare earth ion more strictly from the structure of the unit cell. In the cubic structure β-PbF_2, which we discussed in FOV, the rare earth ions replace the Pb ions located at the center of the face.[16] So there can be three rare earth ions at most in the unit cell, corresponding to the situation of full concentration. If the side length is a, the volume of each rare earth ion is $\overline{V} = a^3/3$. In fact, this concentration may not be 100%, which corresponds to stoichiometric material, for example the concentration q, thus $\overline{V} = (a^3/3)/q$ in β-PbF_2. For oxyfluoride vitroceramics in particular, all reported work has proved that rare earth ions are enriched into the nanophase β-PbF_2 nanocrystal. If we consider that the total crystallized volume ratio of nanophase β-PbF_2 nanocrystal relative to the whole material is η in FOV nanophase oxyfluoride vitroceramics, we have $\overline{V} \cdot \eta = (a^3/3)/q$. We suppose the distance between the nearest ions in the unit cell to be R_0. According to the cubic structure of β-PbF_2, it can be known that Pb ions are positioned at the place of the 8-vertex angle and the 6-center of face. According to reported work,[16] we can know that the rare earth ions replace the Pb ions to locate at the center of the face.[16] The nearest distance R_0 between rare earth ions, after Er replaces Pb in FOV, is the distance between the nearest center of face. If the side length is a, we can obtain that $R_0 = \sqrt{2}a/2$ in β-PbF_2. We can then calculate the real ion distance through the expression of q by $\overline{V}$, a, η and the formula of stoichiometric material $R^3 = R_0^3 \cdot (1/q)$.[20] Thus formula (9) can be easily obtained for oxyfluoride vitroceramics with the nanophase β-PbF_2 cubic structure, in which η is the total crystallized volume ratio of FOV:

$$\begin{aligned} R^3 &= \frac{3\overline{V} \cdot \eta}{a^3} \cdot R_0^3 = \frac{3\sqrt{2}}{4}\overline{V} \cdot \eta = 1.061 \times \overline{V} \cdot \eta \\ &= 1.061 \times \frac{2\eta}{(N_{\mathrm{D}} + N_{\mathrm{A}})}. \end{aligned} \tag{9}$$

Note that formula (4) is different from the formulas (7)–(9) in that the volume of each ion is expressed by the product of two different ion concentrations. But in this paper we prove that using the sum of two kinds of ion concentrations to express $\overline{V}$ is more suitable for FOV material. The experimental dynamic range of intensity reversal in Er(0.05)Yb(9.5):FOV is 845.63 which is close to the Σ of Er(0.5)Yb(9.5):FOV. This result indicates that the energy transfer rates, which play an important role in the intensity reversal

phenomenon, of these two materials should be close, because under the same experimental conditions the same kinds of rare earth ions and the same kinds of hosts should possess similar spontaneous emission rates and nonradiative multiphonon relaxation rates. As has been discussed above, a similar rate of energy transfer means that the interacting ion distance of the two materials should be close. Considering the concentrations of the two materials, it is easy to find that the inversely proportional relationship between R^3 and the sum of two kinds of rare earth ion concentrations of our formulas (8) and (9)[9,11] is closer to the experimental phenomenon than that between R^3 and the product of two kinds of rare earth ion concentrations.[10]

Next we take ErP_5O_{14} and $Er_{0.1}La_{0.9}P_5O_{14}$ as examples to verify the correctness of the method.[21] ErP_5O_{14} corresponds to full concentration material and $q = 100\%$, and the nearest distance between Er^{3+} is known as 0.519 nm. The density of the material is 3.725 g/cm^3. Thus according to the molar mass and Avogadro constant, the number of rare earth ions per unit volume can be achieved. Then the distance results of the methods which correspond to formulas (4)–(7) are obtained and listed in the first line of Table 2. We can note that the calculated distance R of Eq.(4) is longer than the real distance, and the results of the other three methods are shorter than the real distance. That is to say, all of these methods have their own limitations in dealing with real materials. In particular, in discussing the energy transfer rates, these deviations of R can lead to big errors.

Another example is $Er_{0.1}La_{0.9}P_5O_{14}$ which is of non-full concentration material. According to the equation $R^3 = R_0^3 \cdot (1/q)$ and $R_0 \approx 0.519$ nm we can obtain the real rare earth ion distance which is 1.118 nm. Like the processes we discussed above for PbF_2, we can use $V_{\mathrm{unit-cell}}$ and N to express concentration q, where $V_{\mathrm{unit-cell}}$ is the volume of the unit cell[21] and N is the number of rare earth ions per unit volume. There are four rare earth ions per unit cell,[21] so we can obtain

$$q = 4/(N \cdot V_{\mathrm{unit-cell}}). \tag{10}$$

By using the method of formula (10) the calculated distance is 1.101 nm, listed in the second line of Table 2, which is very close to the real distance 1.118 nm. But we can find from Table 2 that all of the results of other methods, which correspond to formulas (4)–(7), are significantly different from 1.118 nm. So our method is more suitable for calculating rare earth ion distance in non-full concentration material than other methods. Meanwhile, the rare earth ion distance R in ErP_5O_{14} is recalculated based on formula (10), the known $V_{\mathrm{unit-cell}}$, calculated N and $R^3 = R_0^3 \cdot (1/q)$. The obtained results are $q = 100\%$ and $R = 0.519$ nm. The result of ErP_5O_{14} recalculated by our method is perfectly coincident with the real nearest rare earth ion distance $R_0 = 0.519$ nm. This proves that our method is an accurate method to calculate distance R.

Table 2. Calculated distance between rare earth ions with different methods. The units are nm.

samples	$R^{(4)}_{\mathrm{product}}$	$R^{(5)}_{\mathrm{cube}}$	$R^{(6)}_{\mathrm{body\ center}}$	$R^{(7)}_{\mathrm{face\ center}}$	$R_{\mathrm{this\ paper}}$	$R_{\mathrm{true\ value}}$
ErP_5O_{14}	0.7747	0.3871	0.4224	0.4345	0.5190	0.519
$Er_{0.1}La_{0.9}P_5O_{14}$	1.643	0.8209	0.8957	0.9214	1.101	1.118

The superscripts (4), (5), (6) and (7) indicate the calculated R values corresponding to Eqs.(4), (5), (6) and (7).

6. Results and analysis

Steady values of the solution of Eqs.(1) and (2) at three different total crystallized volume ratios η of Er(0.5)Yb(9.5):FOV, when excited by 378.5 nm and 522.3 nm light respectively, were calculated theoretically by the original energy transfer theory and are listed in lines 6 to 8 in Table 1. It is remarkable from the conventional energy transfer theory that the range of intensity reversal Σ between the red and green fluorescence increases with the rise of η. On the other hand, it is clear that the distance between two ions should decrease with the reduction of η, and the opposite should be true for the energy transfer rate. That is to say, the theoretical result from the original energy transfer theory of the values of Σ and γ increasing with the rise of η is contrary to experiments and common sense. The ranges of intensity reversal Σ of samples doped with erbium at the same concentration and

with ytterbium at different concentrations were studied experimentally.[5,6] It was found that both the values of Σ and γ increase with the rise of the concentration of ytterbium. The samples, fabricated with similar technology, should possess similar total crystallized volume ratios η. This means that the rise of the ion concentration leads to a reduction in the distance between the ions. So the result of the experiment implies that the values of Σ and γ will decrease with the rise of the distance between the ions, in contradiction to the results of the theoretical calculation with the original phonon-assistant energy transfer theory. By analyzing these calculated results, it was found that the main reason for this contradiction is the great contribution of the Yb^{3+} to Er^{3+} back energy transfers, just like the b, b process in Fig.2, which involves the excitation of Er^{3+} ion from the ground level.

In fact, the energy transfer rate $W_p^{(m\to n,k\to i)} \cdot n_m n_k$ equals the multiplication of the energy transfer probability $W_p^{(m\to n,k\to i)}$ and two population probabilities n_m, n_k of the ion's initial levels. Under weak excitation, most particles remain at the ground level, so energy transfers involving the transition from the ground level are especially noteworthy. Through the analysis it was noted that the real energy transfer rate $W_p^{(m\to n,k\to i)} \cdot n_m n_k$ of $\{^4G_{11/2}(Er^{3+}) \to {}^4F_{9/2}(Er^{3+}),\ {}^2F_{7/2}(Yb^{3+}) \to {}^2F_{5/2}(Yb^{3+})\}$, which possesses a large reduced matrix element and a low energy mismatch, is of the order of 1.5×10^{-4} s^{-1} after getting stabilized in Er(0.5)Yb(9.5):FOV. However, the real energy transfer rate of $\{^2F_{5/2}(Yb^{3+}) \to {}^2F_{7/2}(Yb^{3+}),\ {}^4I_{15/2}(Er^{3+}) \to {}^4S_{3/2},{}^2H_{11/2}(Er^{3+})\}$, of which the energy mismatches are up to 8410.7 cm^{-1} and 9253.2 cm^{-1}, is nearly 4.1×10^{-6} s^{-1}. These high speed processes resulting from the anti-Stokes back energy transfer from the ground level of the erbium ion are exactly the cause of the contradiction between the original theoretical results and the experimental ones. So Raman spectroscopy was brought to mind in the study.[7] In Raman spectroscopy, the expression of the intensity ratio of Stokes Raman scattering to anti-Stokes Raman scattering in the quantum theory is different from that in the classical theory. In the quantum theory there is an additional coefficient, $\exp\{hc\tilde{v}_k/kT\}$, where $\tilde{v}_k$ is the wavenumber deviation from the excitation light.[7] This distinction comes from the different transition probabilities between vibration states of the two processes. A similar result was achieved by Prof. Auzel in discussing the Stokes and anti-Stokes phonon sideband excitation fluorescence.[22] Thus the rate between Stokes and anti-Stokes phonon-assistant energy transfer should be different because they are involved in similar emitting and absorbing multiphonon process. So in the following calculation, the coefficient $\exp\{\Delta E/kT\}$ is introduced to improve the phonon-assistant energy transfer theory of Miyakawa and Dexter[12,13] under the unchanged theory of Prof. Kushida.[8] The original Miyakawa and Dexter theories are considered reasonable only for discussing Stokes processes, whereas the rate of anti-Stokes energy transfer should be divided by the introduced coefficient $\exp\{\Delta E/kT\}$, where ΔE is the energy mismatch of the transfer processes. The improvement leads to a significant reduction in the rates of those back energy transfers from Yb^{3+} to Er^{3+} involving the ground level of the erbium ion.

In Table 3, the first six lines list all the energy transfer channels whose transfer probabilities with the original theory W_{ET} are larger than 10^5 s^{-1} or the transfer probabilities with the improved theory W_{ET}-im are larger than 10^4 s^{-1}. It is found that although there are few transfer channels possessing such large transfer probabilities in Er(0.5)Yb(9.5):FOV, the transfer probability of the energy transfer channel $\{^4G_{11/2}(Er^{3+}) \to {}^4F_{9/2}(Er^{3+}),\ {}^2F_{7/2}(Yb^{3+}) \to {}^2F_{5/2}(Yb^{3+})\}$, which is labeled 1–1 in Fig.2, is up to 4.18×10^6 s^{-1} no matter whether the original theory or the improved theory is used. This value of transfer probability is 10 to 100 times larger than that of other energy transfer channels listed in Table 3. It is this very energy transfer channel in Er(0.5)Yb(9.5):FOV that makes the particles excited to the $^4G_{11/2}$ level depopulate directly to the $^4F_{9/2}$ level, and jump over the $^4S_{3/2}$ level, which causes the fluorescence intensity reversal phenomenon.[23–33]

Comparing the energy transfer results calculated with the original theory with the values obtained with the improved theory in Table 3, we can note that under the original theory the transfer rates of those back energy transfers, which involve the ground level of Er^{3+} as the initial level and possess large energy mismatch, are too large and not negligible, such as the channel b–b in Fig.2. Note that the original energy transfer probabilities W_{PET} of these back energy transfer channels, which are listed in the 7^{th} to 19^{th} lines of the 4^{th} column of Table 3, are indeed smaller than other channels which possess much

smaller energy mismatch. But during the simulation, the real energy transfer rate is $W_{\rm PET} \times N_{\rm Er} \times N_{\rm Yb}$, which includes the product with population probabilities of the ions' initial levels. Through the 8$^{\rm th}$ column of Table 3 we find that these real transfer rates of the above back energy transfer channels, which originate from one ion's ground state and possess very large energy mismatch, are too fast in comparison with other channels. For example, it seems impossible for the anti-Stokes energy transfer channel $\{^2F_{5/2}({\rm Yb}^{3+}) \rightarrow {}^2F_{7/2}({\rm Yb}^{3+}),\ {}^4I_{15/2}({\rm Er}^{3+}) \rightarrow {}^4F_{9/2},\ {}^2H_{11/2}({\rm Er}^{3+})\}$, of which the energy mismatches are up to 5357.9 cm^{-1} and 9253.2 cm^{-1}, to absorb enough energy through the phonons to compensate the big gap to have a real energy transfer rate of 6.9.$\times10^{-6}$ s^{-1} and 4.14.$\times10^{-6}$ s^{-1}, because the real energy transfer rate of $\{^4G_{11/2}({\rm Er}^{3+}) \rightarrow {}^4F_{9/2}({\rm Er}^{3+}),\ {}^2F_{7/2}({\rm Yb}^{3+}) \rightarrow {}^2F_{5/2}({\rm Yb}^{3+})\}$, which possesses a large reduced matrix element and a low energy mismatch, is 1.5×10^{-4} s^{-1}. Thus the improved rates $W_{\rm PET}$-im are more reasonable. These anti-Stokes energy transfer channels should have much lower transfer rates as shown in the last column in Table 3.

Table 3. The energy transfer rates between the Er^{3+} ion and the Yb^{3+} ion in Er(0.5)Yb(9.5): FOV when the total crystallized volume ratio in the glass ceramics is 22.6%.

Er^{3+}		energy mismatch /cm^{-1}	$W_{\rm PET}$/s^{-1}	$W_{\rm PET}$-im/s^{-1}	$N^{\rm b}$ (initial level)	$N^{\rm b}$-im (initial level)	$W_{\rm PET}\times N_{\rm Er}\times N_{\rm Yb}$/s^{-1}	$W_{\rm PET}$-im$\times N_{\rm Er}$-im$\times N_{\rm Yb}$-im/s^{-1}
initial level	final level							
$^4G_{11/2}$[a]	$^4F_{9/2}$	478.53	4.18×10^{6}	4.18×10^{6}	3.58×10^{-11}	3.58×10^{-11}	1.50×10^{-4}	1.50×10^{-4}
$(^2G^4F^2H)_{9/2}$[a]	$^4F_{9/2}$	–1330.3	9.91×10^{3}	1.68×10^{1}	3.29×10^{-11}	3.71×10^{-11}	3.26×10^{-7}	6.23×10^{-10}
$^4I_{11/2}$	$^4I_{15/2}$	–409.91	3.97×10^{5}	5.56×10^{4}	5.28×10^{-7}	2.41×10^{-7}	2.10×10^{-1}	1.34×10^{-2}
$^4F_{3/2}$	$^4I_{11/2}$	–416.54	1.34×10^{5}	1.82×10^{4}	2.46×10^{-12}	5.89×10^{-12}	3.30×10^{-7}	1.07×10^{-7}
$^4F_{7/2}$	$^4I_{9/2}$	–414.18	9.76×10^{4}	1.34×10^{4}	5.90×10^{-13}	6.85×10^{-13}	5.76×10^{-8}	9.18×10^{-9}
$^4G_{9/2}$	$^4F_{9/2}$	1526.8	1.73×10^{5}	1.73×10^{5}	1.71×10^{-16}	7.27×10^{-19}	2.96×10^{-11}	1.26×10^{-13}
$^4I_{15/2}$	$^4I_{13/2}$	3361.2	5.85×10^{2}	5.85×10^{2}	6.70×10^{-7}	1.79×10^{-7}	3.92×10^{-4}	1.05×10^{-4}
$^4I_{15/2}$	$^4I_{11/2}$	–297.56	3.13×10^{5}	7.52×10^{4}	6.70×10^{-7}	1.79×10^{-7}	2.10×10^{-1}	1.35×10^{-2}
$^4I_{15/2}$	$^4I_{9/2}$	–2543.4	7.82×10^{1}	3.94×10^{-4}	6.70×10^{-7}	1.79×10^{-7}	5.24×10^{-5}	7.05×10^{-11}
$^4I_{15/2}$	$^4F_{9/2}$	–5357.9	1.03×10^{1}	7.09×10^{-11}	6.70×10^{-7}	1.79×10^{-7}	6.90×10^{-6}	1.27×10^{-17}
$^4I_{15/2}$	$^4S_{3/2}$	–8410.7	6.78×10^{-2}	2.05×10^{-19}	6.70×10^{-7}	1.79×10^{-7}	4.54×10^{-8}	3.67×10^{-26}
$^4I_{15/2}$	$^2H_{11/2}$	–9253.2	6.18×10^{0}	3.29×10^{-19}	6.70×10^{-7}	1.79×10^{-7}	4.14×10^{-6}	5.89×10^{-26}
$^4I_{15/2}$	$^4F_{7/2}$	–10593	1.85×10^{-2}	1.60×10^{-24}	6.70×10^{-7}	1.79×10^{-7}	1.24×10^{-8}	2.86×10^{-31}
$^4I_{15/2}$	$^4F_{5/2}$	–12284	8.91×10^{-4}	2.31×10^{-29}	6.70×10^{-7}	1.79×10^{-7}	5.97×10^{-10}	4.13×10^{-36}
$^4I_{15/2}$	$^4F_{3/2}$	–12709	3.18×10^{-4}	1.07×10^{-30}	6.70×10^{-7}	1.79×10^{-7}	2.13×10^{-10}	1.92×10^{-37}
$^4I_{15/2}$	$(^2G^4F^2H)_{9/2}$	–14717	6.81×10^{-5}	1.51×10^{-35}	6.70×10^{-7}	1.79×10^{-7}	4.56×10^{-11}	2.70×10^{-42}
$^4I_{15/2}$	$^4G_{11/2}$	–16567	2.90×10^{-3}	9.03×10^{-38}	6.70×10^{-7}	1.79×10^{-7}	1.94×10^{-9}	1.62×10^{-44}
$^4I_{15/2}$	$^4G_{9/2}$	–17565	4.28×10^{-6}	1.11×10^{-42}	6.70×10^{-7}	1.79×10^{-7}	2.87×10^{-12}	1.99×10^{-49}
$^4I_{15/2}$	$^2K_{15/2}$	–18223	1.26×10^{-5}	1.39×10^{-43}	6.70×10^{-7}	1.79×10^{-7}	8.44×10^{-12}	2.49×10^{-50}

[a] The first two lines list two energy transfer channels which contribute more to the color reversal phenomenon, and the Yb^{3+} ion is excited from the ground state $^2F_{7/2}$ to the excited state $^2F_{5/2}$. From the third line to the sixth line, there are four energy transfer channels which possess large transfer probabilities $W_{\rm PET}$ and $W_{\rm PET}$(-im). From the seventh line to the end of the table, there are back energy transfer channels which involve the ground level of the Er^{3+} ion as the initial level, and the initial level of the Yb^{3+} ion is the excited state $^2F_{5/2}$.

[b] The columns of N and N-im, which correspond to the results calculated with the original theory and the improved theory respectively, list the population probabilities of the corresponding initial levels when the sample is excited by 378 nm–0.3 mW light and the fluorescence system becomes stable. The first six numbers of the N and N-im columns are the population probabilities of Er^{3+} for the energy transfer while the population probability of the initial Yb^{3+} level is nearly 1. The other numbers N and N-im are population probabilities of Yb^{3+} for back energy transfer while the population probability of the initial Er^{3+} level is nearly 1.

In Table 3, the third column lists the energy mismatch between donor and acceptor transitions. The negative numbers in this column correspond to anti-Stokes processes, where the transition energy of the donor is smaller than that of the acceptor. The $W_{\rm PET}$ column lists the phonon-assisted energy transfer rates calculated by the original theory. The $W_{\rm PET}$-im column lists the phonon-assisted energy transfer rates calculated by our improved theory which introduced the $\exp\{\Delta E/kT\}$ factor. The last two columns are the results of real transfer rates, which equal the products of $W_{\rm PET}$(-im) or $W_{\rm PET}$ and the population probabilities of the two ions' initial levels, whether we consider the introduced factor or not.

Based on general principles, the fluorescence intensity can be expressed by

$$I_i/N = n_i A_{ij} h\upsilon, \tag{11}$$

where I_i is the fluorescence intensity of the luminescence level i, N is the particle number density of the unit volume, n_i the population probability, $h\upsilon$ the transition energy, and A_{ij} the spontaneous emission rate from level i to level j. Improved theoretical values of fluorescence intensities of $^4S_{3/2}$ and $^4F_{9/2}$ as well as values of α, γ and Σ for different samples are obtained, as listed in Table 1.

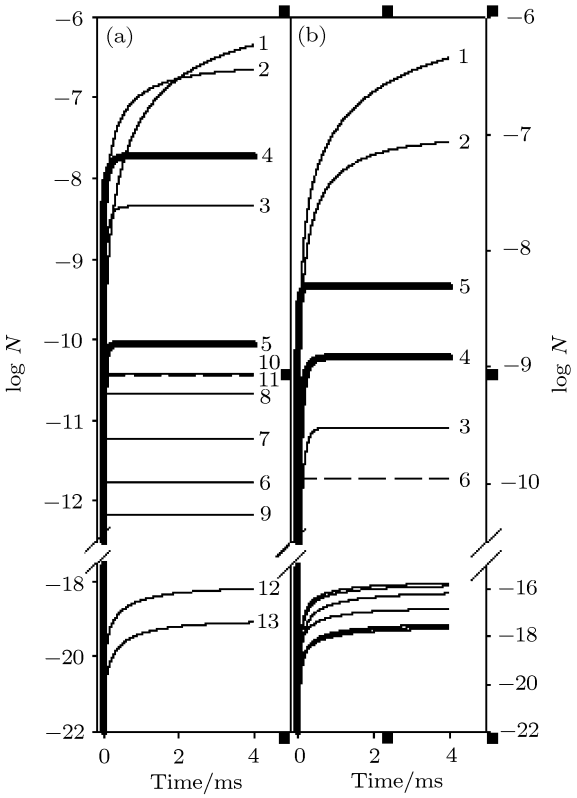


Fig.3. The improved theory curves of the Er^{3+} level population probabilities vs. time when Er(0.5)Yb(9.5):FOV is excited by 378.5 nm light (a) and 522.3 nm light (b). The η is 22.6%. The number near the curve represents the excited level of the Er^{3+} ion from small to large energies.

Figure 3 shows the improved theoretical results of Er(0.5)Yb(9.5):FOV when the total crystallized volume ratio η equals 22.6%. Figure 4 shows the improved theoretical results of Er(0.5):FOV.

It can be clearly seen for Er(0.5):FOV from Fig.4(a) that the population probability of $^4S_{3/2}$ is higher than that of $^4F_{9/2}$ after becoming stabilized. Using Eq.(3) the value of $\gamma = 0.166$ can be obtained, which is basically consistent with the experimental value 0.085. Also, the value of $\alpha = 6.108$ can be calculated from Fig.4(b), in agreement with the experimental result $\alpha = 10.95$. Thus the dynamic range of intensity reversal $\Sigma = \alpha \times \gamma$ is 1.015. The experimental value of Σ is 0.932. These results indicate that the theory agrees very well with the experiment for the sample Er(0.5):FOV.

Figure 3(a) shows improved theoretical results of Er(0.5)Yb(9.5):FOV when the total crystallized volume ratio η equals 22.6% and the sample is excited by 378.5 nm light. We can find that the population probability of level $^4F_{9/2}$ is higher than that of $^4S_{3/2}$, which is very different from Er(0.5):FOV. Considering Eq.(3) further, the intensity of red fluorescence is stronger than that of green fluorescence under this condition, which is in good agreement with the experimental results. For the Yb^{3+}-undoped sample, the population probability of level $^4F_{9/2}$ mainly comes from the upper level $^4S_{3/2}$ through nonradiative multiphonon relaxation no matter whether the excitation wavelength is 378.5 nm or 522.3 nm. But for the sample co-doped with Yb^{3+}, the population probability of level $^4F_{9/2}$ will increase rapidly through the energy transfer channel $\{^4G_{11/2}(Er^{3+}) \rightarrow {}^4F_{9/2}(Er^{3+}),\ {}^2F_{7/2}(Yb^{3+}) \rightarrow {}^2F_{5/2}(Yb^{3+})\}$, as is shown in Fig.2.[23−33] The probability $W_p^{(m\rightarrow n,k\rightarrow i)}$ of this channel is up to 4.18×10^6 and is greater than that of multiphonon relaxation in Er(0.5)Yb(9.5):FOV. So it can be found from Fig.3(a) that the change shown on the curve of level $^4F_{9/2}$ is faster and is stabilized more quickly than the curve of $^4S_{3/2}$. Also, the stabilized population probability of the $^4F_{9/2}$ level is also higher than that in Fig.4 because of this rapid energy transfer channel. Improved theoretical results of the unusual intensity reversal ratio $\gamma = 144.2$ and the common intensity ratio $\alpha = 6.141$ are obtained, and are basically consistent with the experiment. The improved theoretical result of the range of intensity reversal $\Sigma = \alpha \times \gamma$ is 885.7, which agrees perfectly with the experimental calibrated results.

In Table 1, lines 11 and 12 are the improved theoretical results when the η of Er(0.5)Yb(9.5):FOV is assigned to 10% and 16%, respectively. After the introduction of the $\exp\{\Delta E/kT\}$, it is noted that the range Σ of intensity reversal decreases with the rise of the crystallized volume ratio, which coincides with experiment and is quite different from the results without considering the coefficient $\exp\{\Delta E/kT\}$. Meanwhile, through calculation and comparing the results

from line 6 to line 8 in Table 1, we cannot even find an appropriate crystallized volume ratio with the original theory to correspond to the experiment in a wider range than that of 2%–30% proved by relative research,[18,19] if we do not introduce this coefficient $\exp\{\Delta E/kT\}$. Meanwhile, with the improved theory, it was found that when the total crystallized volume ratio in the glass ceramics of Er(0.05)Yb(9.5):FOV is 21.8%, the value of Σ is 837.0, which is coincident with the experimental result shown in Table 1. This total crystallized volume ratio is similar to the value 22.6% of Er(0.5)Yb(9.5):FOV and agrees with the same material manufacture processes of the two materials.

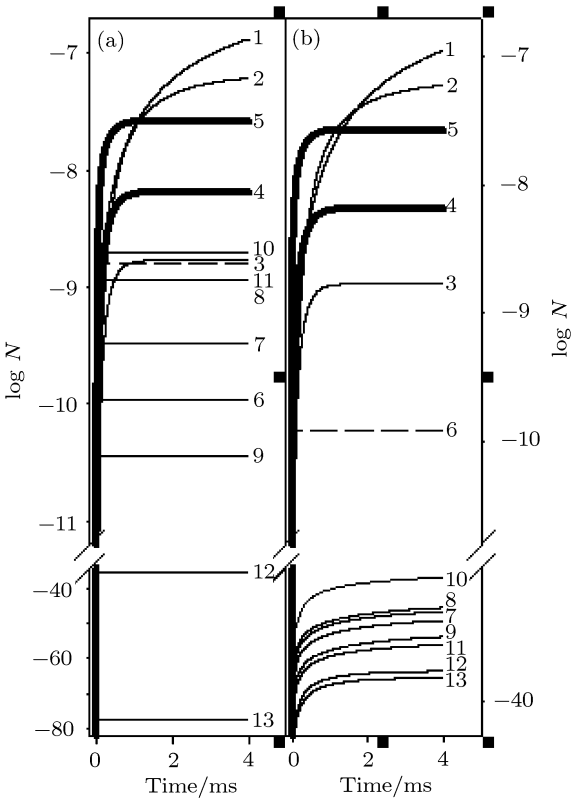


Fig.4. The improved theoretical curves of the Er^{3+} level population probabilities vs. time when Er(0.5):FOV is excited by 378.5 nm light (a) and 522.3 nm light (b). The number near the curve represents the excited level of the Er^{3+} ion from small to large energies.

In order to confirm our improvement on the anti-Stokes energy transfer theory, the fluorescence behavior of Er(0.5)Yb(9.5):FOV when the sample is excited by 646.7 nm red light is studied by experiments and by both the improved and original anti-Stokes energy transfer theories. First, we measured the emission spectra of Er(0.5)Yb(9.5):FOV from 630 nm to 850 nm when the sample was excited by 646.7 nm red light, as is shown in Fig.5. The relative fluorescence emission intensities (the integral emission area which has deduced noise) of $^4I_{9/2}$ and $^4F_{9/2}$ are $1.763.\times10^6$ and 5.226×10^8, thus the experimental ratio of the two intensities is $3.373.\times10^{-3}$. Then steady values of the solution of Eqs.(1) and (2) of Er(0.5)Yb(9.5):FOV, when excited by 646.7 nm light, were calculated theoretically both by the improved and original energy transfer theories. Our improved theoretical results of the population probabilities of $^4I_{9/2}$ and $^4F_{9/2}$ are $2.6142.\times10^{-9}$ and 1.0806×10^{-8}. Considering Eq.(11) further, the improved theoretical fluorescence emission intensity ratio of two levels is 1.4017×10^{-2}. However, the original theoretical population probabilities of $^4I_{9/2}$ and $^4F_{9/2}$ are 2.3923×10^{-9} and 7.4631×10^{-9}, and the original theoretical fluorescence intensity ratio is 1.8573×10^{-2}. Obviously, the results of the improved energy transfer theory are closer to the experimental results, which prove the correctness of the introduction of the coefficient $\exp\{\Delta E/kT\}$.

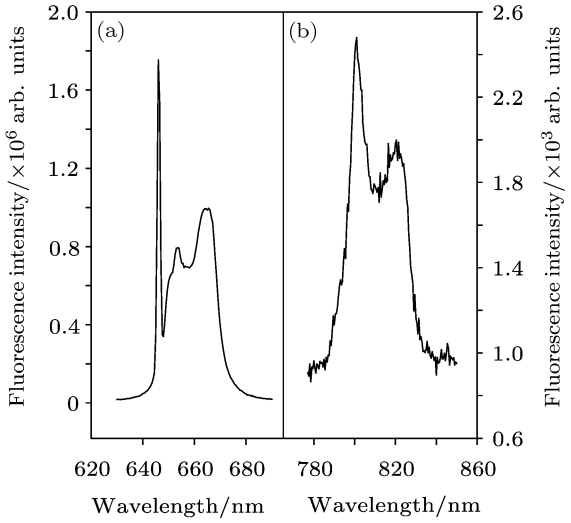


Fig.5. Experimental confirmation of validity of improved energy transfer theory. The calibrated fluorescence emission spectra of the $^4I_{9/2}$ level (a) and the $^4F_{9/2}$ level (b) are a result of 646.7 nm excited light in Er(0.5)Yb(9.5):FOV.

Therefore the above improvement in the theory of anti-Stokes energy transfer between rare earth ions will be significant and indispensable when the photonics of nanomaterials is probed.[1,4,14,15,17–19,23–33] Moreover, plenty of upconversion research, which has been a frontier in past decades, has found experimental support for the idea that the Stokes upconversion process resulting from Stokes energy transfer is obviously larger than the anti-Stokes upconversion pro-

cess resulting from anti-Stokes energy transfer. Our improved anti-Stokes energy transfer theory can also explain the above upconversion phenomena very well.

7. Conclusion

This paper focuses on the introduction of a coefficient, an improvement factor in the intensity ratio of Stokes to anti-Stokes processes in the quantum Raman theory compared to the classical Raman theory, to the calculation of energy transfer rate. The correctness of this improved theory has been proved by experiment. It is found that our improvement in the theory of anti-Stokes energy transfer between rare earth ions is significant and indispensable when the photonics of nanomaterials is probed.

Acknowledgements

The authors would like to thank Prof. Hu Jin-Hao at Beijing Normal University, Prof. Wu Ping-Xiang at Fuzhou University, Prof. Francois Auzel in France, Prof. He Chen-Juan at Beijing Normal University, Prof. Wu Ying-Nan at Peking University, Prof. Zhao Sui-Tang at Peking University, and Prof. Wang Ya-Fei at Beijing Normal University for useful help.

References

[1] Yang G Z *National Natural Science Foundation of China 1995 Optical Physics Science* (Beijing: Science Press) (in Chinese)
[2] Prasad P N 2004 *Nanophotonics* (N. J. Hoboken, Wiley-Interscience)
[3] Xiao S G, Yang X L and Liu Z W 2002 *Chin. Phys.* **11** 188
[4] Feynman R P 1960 *Engineering and Science* **23** 22
[5] Chen X B, Song Z F, Hu L L, Zhang J J and Wen L 2007 *Opt. Lett.* **32** 2019
[6] Chen X B, Song Z F, Hu L L, Zhang J J, Wang C, Wen L and Li S 2007 *Opt. Express* **15** 13421
[7] Ewen S and Geoffrey D 2005 *Modern Raman Spectroscopy: a Practical Approach* (Hoboken: NJ, John Wiley)
[8] Kushida T 1973 *J. Phys. Soc. Jpn.* **34** 1318
[9] Tsuda M, Soga K, Inoue H, Inoue S and Makishima A 1999 *J. Appl. Phys.* **85** 29
[10] Chen C Y, Petrin R R, Yeh D C, Sibley W A and Adam J L 1989 *Opt. Lett.* **14** 432
[11] Tsuda M, Soga K, Inoue H and Makishima A 2000 *J. Appl. Phys.* **88** 1900
[12] Miyakawa T and Dexter D L 1970 *Phys. Rev.* B **1** 70
[13] Miyakawa T and Dexter D L 1970 *Phys. Rev.* B **1** 2961
[14] Carnall W T, Fields P R and Rajnak K 1968 *J. Chem. Phys.* **49** 4424
[15] Wang Y H and Ohwaki J 1993 *Appl. Phys. Lett.* **63** 3268
[16] Beggiora M, Reaney I M and Islam M S 2003 *Appl. Phys. Lett.* **83** 467
[17] Reisfeld R 1977 *Lasers and Excited States of Rare-earths* (Berlin, Heidelberg, New York: Springer-Verlag)
[18] Quimby R S, Tick P A, Borrelli N F and Cornelius L K 1998 *J. Appl. Phys.* **83** 1649
[19] Mortier M and Auzel F 1999 *J. Non-cryst. Solids* **256–257** 361
[20] Zhang S Y 1991 *Theory of Rare Earth Spectroscopy* (Changchun: Jilin Science Press) (in Chinese)
[21] Katrusiak A and Kaczmarek F 1995 *Cryst. Res. Technol.* **30** 501
[22] Auzel F 1976 *Phys. Rev.* B **13** 2809
[23] Schaudel B, Goldner P, Prassas M and Auzel F 2000 *Journal of Alloys and Compounds* **300** 443
[24] Su F N and Deng Z D 2006 *Chin. Phys.* **15** 1096
[25] Xiao S G, Ding Q L, Zhang X H, Xia Y Q and Liu Z W 2006 *Acta Phys. Sin.* **55** 5140 (in Chinese)
[26] Wang X, Shan G Y, An L M, Chao K F, Zeng Q H, Chen B J and Kong X G 2004 *Acta Phys. Sin.* **53** 1972 (in Chinese)
[27] Yang H G, Dai Z W and Zu N N 2007 *Chin. Phys.* **16** 1650
[28] Auzel F 2004 *Chem. Rev.* **104** 139
[29] Auzel F, Pecile D and Morin D 1975 *J. Electro. Soc.* **122** 101
[30] Chen X Y and Luo Z D 1998 *Acta Phys. Sin.* **7** 773 (Overseas Edition)
[31] Niu Y, Wang Z M, Liu Y C, Yin Y S and Yuan D R 2007 *Acta Phys. Sin.* **56** 2968 (in Chinese)
[32] Chen X B, Song Z F, Sun Y G, Zhang G Y, Yang Z R and Nie Y X 1999 *Acta Phys. Sin.* **8** 216 (Overseas Edition)
[33] Chen D Q, Wang, Y S and Yu Y L 2007 *Opt. Lett.* **32** 3068